J|A|C|S
ARTICLES
Published on Web 02/10/2006

Pyridine−Ag_{20} Cluster: A Model System for Studying Surface-Enhanced Raman Scattering

Linlin Zhao, Lasse Jensen,* and George C. Schatz

Contribution from the Department of Chemistry, Northwestern University, 2145 Sheridan Road, Evanston, Illinois 60208-3113

Received August 17, 2005; E-mail: l.jensen@chem.northwestern.edu

Abstract: This work presents a detailed analysis of enhanced Raman scattering of the pyridine−Ag_{20} model system using time-dependent density functional theory. A consistent treatment of both the chemical and electromagnetic enhancements (EM) is achieved by employing a recently developed approach based on a short-time approximation for the Raman cross section. A strong dependence of the absolute and relative intensities on the binding site and excitation wavelength is found. The analysis of the Raman scattering cross sections shows the importance of different contributions to the enhancements, including static chemical enhancements (factor of 10), charge-transfer enhancements (10^3), and EM enhancements (10^5). The largest enhancement found (10^5-10^6) is due to the EM mechanism, with a small contribution from the chemical interaction. This suggests that the enhanced Raman scattering due to atomic clusters is comparable to findings on single nanoparticles. A combination of information about the vibrational motion and the local chemical environment provides a simple picture of why certain normal modes are enhanced more than others.

I. Introduction

Ordinarily weak, Raman scattering cross sections can be greatly enhanced when the analyte molecule is absorbed on noble metallic surfaces and in particular on silver nanoparticles. This phenomenon is generally referred to as surface-enhanced Raman scattering (SERS), and it has opened the possibilities of using Raman techniques for single molecule detection.[1−4] The requirement for single molecule detection using Raman spectroscopy is that the cross section is enhanced by a factor of $10^{14}-10^{15}$. These huge enhancements have been achieved using silver nanoparticles or nanoparticle aggregates in conjunction with resonance enhancements due to a molecular electronic transition.[1−3] This stands in contrast to the traditional 10^4-10^6 order of enhancements found on rough surfaces[5−8] or in resonance enhanced Raman spectroscopy.[9] Thus far, most studies have focused on using either rough surfaces or nanoparticles to achieve these large enhancements; however, recent studies by Dickson and co-workers showed that a similar huge enhancement could be obtained by encapsulating small atomic Ag clusters in dendrimer and peptide structures.[10]

Although SERS was discovered several decades ago,[11−13] a complete picture of the enhancement mechanism is not available, due to its highly complicated experimental conditions (roughed surfaces, nanoparticle aggregates, etc.). Many mechanisms have been proposed to account for these huge enhancements,[5,8,14] and it is generally accepted that there are three major contributions: (a) changes in the electronic properties of the molecule, (b) resonance enhancements due to either existing excitations in the molecule or newly created metal−molecule charge-transfer excitations, and (c) enhanced local electromagnetic fields due to the excitations in the metal. The first two contributions are generally grouped as chemical enhancements, and the last as electromagnetic (EM) enhancements. For the growing field of single molecule detection, it is important to have a clear understanding of the individual mechanisms and their relative contributions to the overall observed enhancement.

Electronic structure modeling of the molecule−metal cluster interfacial structure and its optical properties on the atomic scale can provide key insights into the type and strength of the bonds between the molecule and the nanoparticles/nanoclusters, the effects of the surface roughness on the atomic scale, the effects of the laser excitation wavelength, and, overall, the nature of the observed Raman enhancement itself. Electronic structure

(1) Nie, S. M.; Emory, S. R. *Science* **1997**, *275*, 1102−1106.
(2) Kneipp, K.; Wang, Y.; Kneipp, H.; Perelman, L. T.; Itzkan, I.; Dasari, R. R.; Feld, M. S. *Phys. Rev. Lett.* **1997**, *78*, 1667−1670.
(3) Xu, H.; Bjerneld, E. J.; Käll, M.; Börjesson, L. *Phys. Rev. Lett.* **1999**, *83*, 4357−4360.
(4) Michaels, A. M.; Nirmal, M.; Brus, L. E. *J. Am. Chem. Soc.* **1999**, *121*, 9932−9939.
(5) Otto, A. Surface enhanced Raman scattering: "classical" and "chemical" origins. In *Light Scattering in Solids*; Cardona, M., Güntherodt, G., Eds.; Topics of Applied Physics 54; Springer: Berlin, 1984; Vol. IV.
(6) Moskovits, M. *Rev. Mod. Phys.* **1985**, *57*, 783−826.
(7) Schatz, G. C. *Acc. Chem. Res.* **1984**, *17*, 370−376.
(8) Campion, A.; Kambhampati, P. *Chem. Soc. Rev.* **1998**, *27*, 241−250.
(9) Asher, S. A. *Annu. Rev. Phys. Chem.* **1988**, *39*, 537−588.
(10) Peyser-Capadona, L.; Zheng, J.; Gonzalez, J. I.; Lee, T.-H.; Patel, S. A.; Dickson, R. M. *Phys. Rev. Lett.* **2005**, *94*, 058301(1)−058301(4).
(11) Fleischman, M.; Hendra, P. J.; McQuillan, A. J. *Chem. Phys. Lett.* **1974**, *26*, 163−166.
(12) Jeanmaire, D. L.; Van Duyne, R. P. *J. Electroanal. Chem.* **1974**, *84*, 1−20.
(13) Albrecht, M. G.; Crieghton, J. A. *J. Am. Chem. Soc.* **1977**, *99*, 5215−5217.
(14) Schatz, G. C.; Van Duyne, R. P. Electromagnetic mechanism of surface enhanced spectroscopy. In *Handbook of Vibrational Spectroscopy*; Chalmers, J. M., Griffiths, P. R., Eds.; Wiley & Sons: New York, 2002; Vol. 1.

methods are ideal tools but are limited by high computational demands. For this reason, most electronic structure studies have adopted small silver clusters to mimic metal surfaces.[15−20] In addition, most have considered static Raman scattering, and therefore only the chemical enhancements have been modeled. Other electronic structure approaches have included two-state resonance Raman models,[21−23] jellium models,[24] and time-dependent Hartree−Fock calculations for molecules near metal clusters.[25−27] For an overview of earlier models, the reader is referred to the review by Moskovits.[6]

In this article, we adopt a 20-atom silver cluster and present a detailed analysis of the enhanced Raman scattering of pyridine interacting with this cluster using a recently developed time-dependent density functional theory (TDDFT) method, based on a short-time approximation to the Raman scattering cross section.[28,29] This short-time approximation makes it possible to calculate both normal Raman scattering (NRS) and resonance Raman scattering (RRS) intensities from the geometrical derivatives of the frequency-dependent polarizability (real or complex). Photodepletion studies of small silver clusters (2−21 atoms) embedded in rare-gas matrixes have shown that the absorption spectrum of Ag_{20} cluster in an argon matrix is dominated by a broad peak with a maximum at 3.70 eV and a weaker peak at 3.97 eV.[30] Although this broad absorption feature cannot be considered as a true collective excitation due to the small size of the cluster, it can be considered as a microscopic analogue to the plasmon excitation observed in nanoparticles. Effectively, it should behave quite similarly and produce an enhanced local electric field if the incident light is at resonance. By adopting this model system, we show that a consistent treatment of both the EM and the chemical enhancements can be achieved using our recently developed approach. We show that the Raman spectrum, both absolute and relative intensities, depends not only on the local chemical environment of the molecule−metal binding site, but also on the incident excitation wavelength. Different contributions to the enhancements are analyzed and are found to be of the order of static chemical enhancements (factor of 10) < charge-transfer enhancements (10^3) < EM enhancements (10^5). The degree of enhancements for the important normal modes can be rationalized by their vibrational motion and the local chemical environment of the molecule. This provides a fairly simple visual picture showing key information about the enhancements.

II. Computational Details

Absolute Raman intensities are presented here as the differential Raman scattering cross section. For Stokes scattering with an experimental setup of a 90° scattering angle and perpendicular plane-polarized light, the cross section is given by[31]

$$\frac{d\sigma}{d\Omega} = \frac{\pi^2}{\epsilon_0^2}(\tilde{\nu}_{in} - \tilde{\nu}_p)^4 \frac{h}{8\pi^2 c\tilde{\nu}_p}[45\bar{\alpha}_p'^2 + 7\gamma_p'^2] \frac{1}{45[1 - \exp(-hc\tilde{\nu}_p/k_B T)]} \quad (1)$$

where $\tilde{\nu}_{in}$ and $\tilde{\nu}_p$ are the frequency of the incident light and of the pth vibrational mode, respectively. $\bar{\alpha}_p'$ and γ_p' are the isotropic and anisotropic polarizability derivatives with respect to the vibrational mode p.

The electronic polarizability both on and off resonance is calculated by including a finite lifetime of the electronic excited states using TDDFT, the details of which are described elsewhere.[28,29] The finite lifetime is included phenomenologically by a common damping parameter Γ. Values of Γ are best obtained by fitting absorption data for the molecule (if available); however, the values do not vary a lot between similar molecules in the limit of a short-time approximation. This is a reasonable approximation here since the absorption spectrum of the silver cluster does not show vibrational fine structure. A damping parameter of $\Gamma \approx 0.004$ au (800 cm^{-1}) is what we have found previously to be reasonable,[28,29] and this value is used throughout this article.

All calculations presented in this work have been done using a local version of the Amsterdam Density Functional (ADF) program package.[32,33] The Becke−Perdew (BP86) XC-potential[34,35] and a triple-ζ polarized slater type (TZP) basis set from the ADF basis set library have been used, with the 1s−4p core kept frozen for Ag. The vibrational frequencies and normal modes are calculated within the harmonic approximation. This means that vibrational coupling beyond the harmonic approximation is neglected, and therefore, overtones and Fermi resonances are not included. However, the harmonic approximation seems to be appropriate for the pyridine silver system.[18] For this reason, the BP86 functional has been chosen since it usually gives harmonic frequencies close to experimental results without the use of scaling factors.[36] Full geometry optimization, standard excitation, and frequency calculations for both isolated molecule, metal cluster, and molecule−metal complex have been performed prior to the polarizability calculations. The polarizability derivatives are then calculated by numerical three-point differentiation with respect to the normal mode displacements as described in detail in ref 37. This allows us to selectively study the Raman intensities of the normal modes associated with pyridine. It should be stressed, however, that the normal modes have been obtained for the full system (i.e., including both the silver cluster and the pyridine molecule). Anharmonic corrections to the Raman intensities are neglected since the Raman intensities are calculated within the so-called double harmonic approximation.[31] The double harmonic approximation seems to be fairly accurate for the intensities of the fundamentals especially considering the experimental uncertainties when measuring absolute intensities.[38]

(15) Yang, W.-H.; Schatz, G. C. *J. Chem. Phys.* **1992**, *97*, 3831−3845.
(16) Aroca, R. F.; Clavijo, R. E.; Halls, M. D.; Schlengel, H. B. *J. Phys. Chem. A* **2000**, *104*, 9500−9505.
(17) Cardini, G.; Muniz-Miranda, M. *J. Phys. Chem. B* **2002**, *106*, 6875−6880.
(18) Vivoni, A.; Birke, R. L.; Foucault, R.; Lombardi, J. R. *J. Phys. Chem. B* **2003**, *107*, 5547−5557.
(19) Wu, D. Y.; Hayashi, M.; Lin, S. H.; Tian, Z. Q. *Spectrochim. Acta, Part A* **2004**, *60*, 137−146.
(20) Johansson, P. *Phys. Chem. Chem. Phys.* **2005**, *7*, 475−482.
(21) Lombardi, J. R.; Birke, R. L.; Lu, T.; Xu, J. *J. Chem. Phys.* **1986**, *84*, 4174−4180.
(22) Arenas, J. F.; Woolley, M. S.; Otero, J. C.; Marcos, J. I. *J. Phys. Chem.* **1996**, *100*, 3199−3206.
(23) Lee, M. T.; Wu, D. Y.; Tian, Z. Q.; Lin, S. H. *J. Chem. Phys.* **2005**, *122*, 094719.
(24) Xu, M.; Dignam, M. J. *J. Chem. Phys.* **1992**, *96*, 8000−8011.
(25) Pandey, P. K.; Schatz, G. C. *J. Chem. Phys.* **1984**, *80*, 2959−2972.
(26) Nakai, H.; Nakatsuji, H. *J. Chem. Phys.* **1995**, *103*, 2286−2294.
(27) Corni, S.; Tomasi, J. *J. Chem. Phys.* **2002**, *116*, 1156−1164.
(28) Jensen, L.; Autschbach, J.; Schatz, G. C. *J. Chem. Phys.* **2005**, *122*, 224115.
(29) Jensen, L.; Zhao, L.; Autschbach, J.; Schatz, G. C. *J. Chem. Phys.* **2005**, *123*, 174110.
(30) Fredigo, S.; Harbich, W.; Buttet, J. *Phys. Rev. B* **1993**, *47*, 10706−10715.
(31) Neugebauer, J.; Reiher, M.; Kind, C.; Hess, B. A. *J. Comput. Chem.* **2002**, *23*, 895−910.
(32) ADF: Density Functional Theory (DFT) Software for Chemists. http://www.scm.com (accessed 2005).
(33) te Velde, G.; Bickelhaupt, F. M.; Baerends, E. J.; Fonseca Guerra, C.; van Gisbergen, S. J. A.; Snijders, J. G.; Ziegler, T. *J. Comput. Chem.* **2001**, *22*, 931−967.
(34) Becke, A. D. *Phys. Rev. A* **1988**, *38*, 3098−3100.
(35) Perdew, J. P. *Phys. Rev. B* **1986**, *33*, 8822−8824.
(36) Neugebauer, J.; Hess, B. A. *J. Chem. Phys.* **2003**, *118*, 7215−7225.
(37) Reiher, M.; Neugebauer, J.; Hess, B. A. *Z. Phys. Chem.* **2003**, *217*, 91−103.
(38) Neugebauer, J.; Reiher, M.; Hess, B. A. *J. Chem. Phys.* **2002**, *117*, 8623−8633.

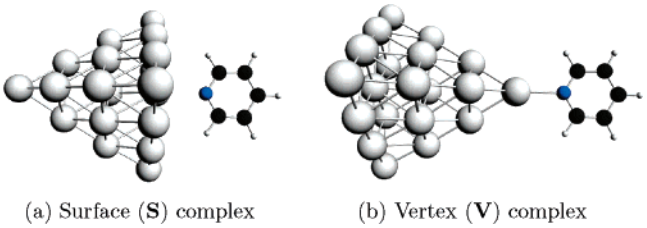

Figure 1. Configurations of the two pyridine−Ag_{20} complexes having C_s symmetry.

III. Results and Discussion

Tetrahedral Ag_{20} is a relaxed fragment of the face-centered cubic (fcc) lattice of bulk silver. Studies using density functional theory (DFT) have shown that this structure is one of the local minima for the Ag_{20} cluster.[39,40] Recently, Wang and co-workers have found that this is the structure Au_{20} possesses by combining photoelectron spectroscopy and relativistic DFT calculations.[41] The unique structure of the Ag_{20} tetrahedron allows us to study two very different binding sites, which we denote as the **S**-complex and the **V**-complex. The former consists of an on-top binding onto one of its four faces, which represents a (111) surface of fcc silver, while the latter consists of binding onto one of its vertexes, which represents an ad-atom site. These two sites, displayed in Figure 1, have been chosen due to their very different local chemical environments. Similar to most previous studies, we assume that pyridine binds to the silver cluster through the nitrogen atom in a perpendicular manner. Here pyridine is oriented so that its *x*-axis is along the Ag−N bond, the *y*-axis is perpendicular out-of-plane, and the *z*-axis is perpendicular in-plane.

A complete list of the optimized geometries and harmonic frequencies is given in the Supporting Information for the structures considered in this work. For both complexes we find imaginary frequencies of magnitude less than 31 cm^{-1}, which is most likely due to a small inaccuracy in the numerical grid.

A. Ground-State Properties. The calculated bond distance between the N atom and the closest silver atom is 2.66 Å for the **S**-complex, whereas it is 2.46 Å for the **V**-complex. For each complex, the bonding energy between pyridine and the silver cluster is analyzed using the extended transition state method developed by Ziegler and Rauk.[42−44] The total bonding energy consists of two major components which are the preparation energy and the interaction energy. The preparation energy is the amount of energy needed to deform the isolated fragments to the structure they have in the complex. This contribution to the energy is negligible here, and we will equate the bonding energy with the interaction energy. The interaction energy can be decomposed into three physical contributions as[45] $\Delta E = \Delta E^{el} + \Delta E^{Pauli} + \Delta E^{orb}$. The first term is the classical electrostatic interaction between the unperturbed charge distributions of the two fragments; the second term is the Pauli repulsion, which represents the destabilization due to interaction between occupied orbitals and accounts for steric repulsion; and the last term is the interaction between occupied and virtual orbitals and accounts for electron pair bond formation, charge transfer, and polarization.[33] The values for these energy contributions have been collected in Table 1 for the two complexes. Basis set superposition errors (BSSE) have been accounted for using the counterpoise method[46] by calculating the bonding energies with respect to the isolated fragments.[33]

Table 1. Decomposition of the Bonding Energy for the Two Complexes[a]

energy terms	**S**-complex	**V**-complex
electrostatic ΔE^{el}	−23.37	−35.81
Pauli repulsion ΔE^{Pauli}	30.64	38.15
orbital interaction ΔE^{orb}	−9.26	−11.53
total binding	−1.99	−9.19
total binding corrected for BSSE	−1.31	−8.87

[a] Energies in kcal/mol.

As we can see, the **S**-complex has a bonding energy of −1.31 kcal/mol compared to −8.87 kcal/mol for the **V**-complex. For both complexes, the BSSE is found to be quite small: 0.68 kcal/mol for the **S**-complex and 0.32 kcal/mol for the **V**-complex. The binding energy is typical for silver interacting with N-heterocycles, but of course, the numbers we calculate are probably uncertain by a few kcal/mol. The bonding interaction for the **V**-complex is stronger, which is in good agreement with its smaller N−Ag bond length. We note that for both complexes the electrostatic energy is not large enough to compensate for the Pauli repulsion, and without the energy contribution from the orbital interaction, the interaction energy would be repulsive by 7.27 and 2.34 kcal/mol for the **S**- and **V**-complexes, respectively. The redistribution of the charge density when forming the complexes has been analyzed by calculating the Voronoi deformation density (VDD) charges.[33] The VDD charges correspond to how much electronic charge is entering or leaving a region of space around the nucleus. We find that 0.11e is transferred from pyridine to the silver cluster for the **S**-complex, whereas 0.13e is transferred for the **V**-complex. A graphical representation of the calculated deformation density $\Delta\rho = \rho^{Ag_{20}-py} - \rho^{Ag_{20}} - \rho^{py}$ for each complex is presented in Figure 2. It is clear to see the flow of density from the pyridine and the central silver atom into the Ag−N bonding region, which agrees well with the overall transfer of charge from pyridine to the silver cluster. For the **S**-complex, we also see enhanced density in the Ag−H bonding region, which obviously is not present for the **V**-complex. This is again in good agreement with the shorter Ag−N bond length found for the **V**-complex. In general, we find that the interactions between the pyridine and the silver cluster are rather weak. One could consider the **S**-complex as a physiosorption complex, whereas the **V**-complex could be considered as a weak chemisorbed complex due to its smaller N−Ag bond length.

B. Electronic Spectra. As mentioned in the Introduction, photodepletion studies[30] have shown that the absorption spectrum of a Ag_{20} cluster embedded in an argon matrix is dominated by a broad peak with a maximum at 3.70 eV. The shift due to the argon matrix was estimated to be a red shift of around 0.24 eV. For the isolated Ag_{20} tetrahedral cluster considered here, the calculated excitation energies in the energy region up to 4

(39) Wang, J.; Wang, G.; Zhao, J. *Chem. Phys. Lett.* **2003**, *380*, 716−720.
(40) Fernández, E. M.; Soler, J. M.; Garzón, I. L.; Balbás, L. C. *Phys. Rev. B* **2004**, *70*, 165403(1)−165403(14).
(41) Li, J.; Li, X.; Zhai, H.-J.; Wang, L.-S. *Science* **2003**, *299*, 864−867.
(42) Zeigler, T.; Rauk, A. *Theor. Chim. Acta* **1977**, *46*, 1−10.
(43) Ziegler, T.; Rauk, A. *Inorg. Chem.* **1979**, *18*, 1558−1565.
(44) Ziegler, T.; Rauk, A. *Inorg. Chem.* **1979**, *18*, 1755−1759.
(45) Bickelhaupt, F. M.; Baerends, E. J. Kohn−Sham density functional theory: predicting and understanding chemistry. In *Reviews in Computational Chemistry*; Lipkowitz, K. B., Boyud, B., Eds.; Wiley-VCH: New York, 2000; Vol. 15.
(46) Boys, S. F.; Bernardi, F. *Mol. Phys.* **1970**, *19*, 553.

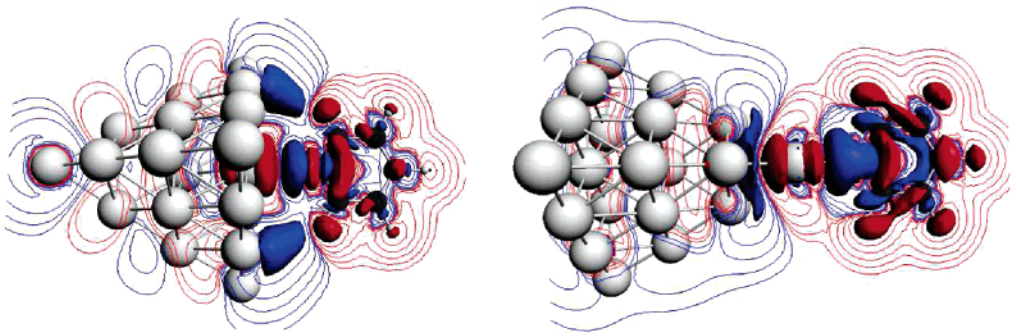

(a) **S**-complex (b) **V**-complex

Figure 2. Calculated deformation density ($\Delta\rho$) isosurface and contour plots for the two complexes. Isosurface value of 0.0004 au with enhanced density in blue and depletion density in red.

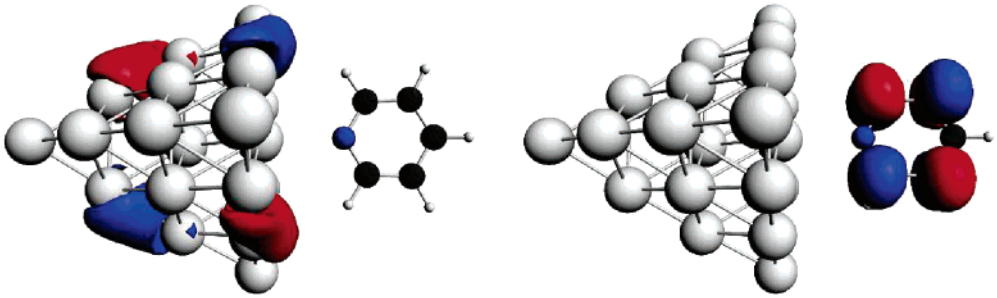

(a) Ag_{20} HOMO (b) Pyridine LUMO+1

Figure 3. Important orbitals involved in the major CT excitation for the **S**-complex shown with an isosurface value of 0.03 au.

eV are dominated by one very strong triple-degenerate excitation at 3.44 eV with an oscillator strength of $f = 7.172$. The calculated results are lower in energy than the experimental results, especially considering the estimated red shift due to the argon matrix. A likely explanation for the differences is that the cluster studied in the experiments possesses a slightly different structure. For the two complexes, the strong excitations are found at 3.33 ($f = 1.186$), 3.35 ($f = 1.393$), and 3.42 ($f = 2.000$) eV for the **S**-complex and at 3.41 ($f = 2.054$), 3.42 ($f = 2.392$), and 3.42 ($f = 2.452$) eV for the **V**-complex. We see an energy splitting of the triple-degenerate excitation due to the lowering of the symmetry for both complexes, although the three excitations are still nearly degenerate for the **V**-complex. The stronger energy splitting for the **S**-complex is most likely due to the interaction between the hydrogens and the silver atoms. The reason for this is that the orbitals involved in these transitions (see Figure 3) are located on the surface of the cluster and are therefore interacting stronger with pyridine in the metal excited state even though the **V**-complex has the stronger interactions in the ground state.

In addition to the changes in the excitations associated with the silver cluster, the presence of a pyridine molecule also creates new charge-transfer (CT) excitations in the energy region below 4 eV. These CT excitations are transitions from the highest occupied orbital (HOMO) of the silver cluster to the lowest unoccupied orbital (LUMO) or LUMO + 1 of the pyridine molecule. The calculated CT excitation energies and oscillator strengths are collected in Table 2. We see that the CT excitations are about 0.5 eV higher for the **S**-complex compared with those for the **V**-complex. This is easily understood if one consider the orbitals involved in the transitions.

Table 2. Calculated Excitation Energies and Oscillator Strengths of Charge-Transfer Excitations for the Two Complexes[a]

		S-complex		**V**-complex	
Ag_{20}	Py	*E*	*f*	*E*	*f*
HOMO →	LUMO	2.16	0.0004	1.44	0.004
HOMO →	LUMO+1	2.63	0.039	1.91	0.0001

[a] Excitation energies in electronvolts.

This is illustrated by Figure 3 where the orbitals are depicted for one selected transition discussed below.

From Figure 3, we see that the HOMO of the Ag_{20} cluster is mainly located in the region where the hydrogens of pyridine are close to the Ag_{20} surface in the **S**-complex. This leads to a destabilization of the LUMO and LUMO + 1 as compared to the **V**-complex, which leads to the higher excitation energies. CT excitations of pyridine absorbed on a Ag(111) surface have been observed by electron energy loss (EELS) experiments to be around 1.4−2.4 eV.[47] However, it has been proposed that EELS is not suitable to observe such weak CT excitations.[48] In fact, by inverse photoemission (IPE) the unresolved LUMO and LUMO + 1 are found to be around 2.9 ± 0.2 eV above the Fermi level.[49] For pyridine on a Cu(111) surface, Wolf and coworkers found the states to be at 3.15 and 3.75 eV above the Fermi level using two photon photoemission (2PPE).[50] Both of these results are significantly higher than the EELS results. The results presented in Table 2 appear to be in good agreement with the EELS results. However, it is well-known that standard TDDFT calculations underestimate CT excitations in weakly

(47) Avouris, P.; Demuth, J. E. *J. Chem. Phys.* **1981**, *75*, 4783−4794.
(48) Zylka, G.; Otto, A. *Surf. Sci.* **2001**, *475*, 118−130.
(49) Otto, A.; Frank, K. H.; Reihl, B. *Surf. Sci.* **1985**, *163*, 140−152.
(50) Zhong, Q.; Gahl, C.; Wolf, M. *Surf. Sci.* **2002**, *496*, 21−32.

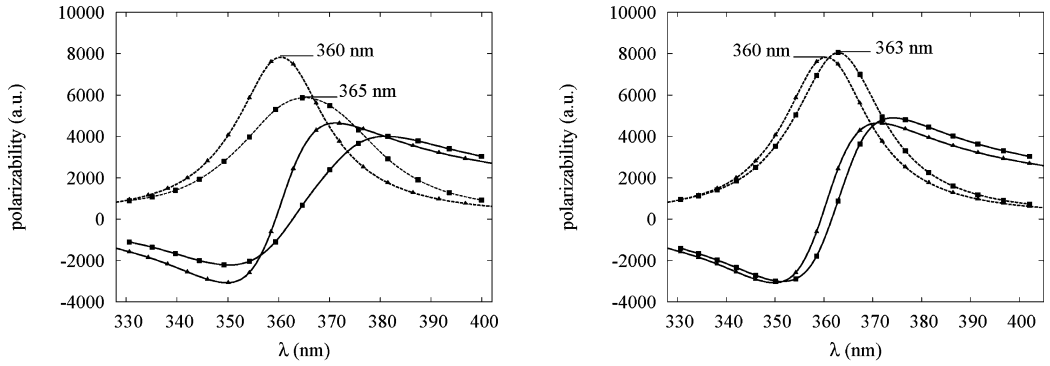

(a) **S**-complex (b) **V**-complex

Figure 4. Calculated real (solid line) and imaginary (dashed line) polarizability of the two py−Ag_{20} complexes and the Ag_{20} cluster as a function of wavelength. Squares denote the complex, and triangles denote the Ag_{20} cluster. Polarizabilities in au and wavelength in nanometers.

Table 3. Calculated Static Electronic Polarizability Components and the Isotropic Polarizability in au

	Ag_{20}	Py	**S**-complex	**V**-complex
α_{xx}	930.6	76.0	1094.5	1126.6
α_{yy}	930.6	35.4	953.4	970.4
α_{zz}	930.6	71.9	974.8	998.0
$\bar{\alpha}$	930.6	61.1	1007.6	1031.6

interacting systems and predict the wrong distance dependence.[51] This is related to a deficiency in the adopted exchange-correlations kernel (usually the adiabatic LDA or GGA). The CT excitation energies then become identical to the orbital differences for orbitals with zero overlap. This is indeed what is found here, and therefore the good agreement with the EELS observation is most likely due to an underestimation rather than a correct description. However, as we will show later, this separation of the CT excitations from the strong excitations around 3.4 eV allows us to probe these two energy regions separately.

C. Polarizabilities. The determination of the polarizability of small metal clusters provides insights into their structures, especially if this is combined with information about the dispersion or electronic excitations.[28,52] A prime example is small alkali metal clusters, where the interplay between accurate theoretical models and experimental results provided a detailed understanding of the electronic configurations and, at least for the smaller clusters, a determination of the ground-state geometries.

The calculated static electronic polarizability components and the isotropic polarizability are listed in Table 3 for the Ag_{20} cluster, the pyridine molecule, and both **S**- and **V**-complexes. Although the static polarizability might have a considerable vibrational contribution, we will only consider the electronic part of the polarizability since this is the part relevant for Raman scattering. We see that for both complexes, the polarizability along the *x*-axis is larger than the sum of the Ag_{20} and pyridine polarizabilities, whereas it is smaller in the other two directions, leading to an isotropic polarizability slightly larger than the sum. These changes in the polarizabilities are consistent with weakly interacting molecular complexes.[53] The fact that the **V**-complex has a larger polarizability in the *x*-direction than the **S**-complex is expected due to its stronger bonding interactions. However, for the **S**-complex the components in the *y*- and *z*-directions are more affected than the **V**-complex. The reason for this is most likely the interactions of the H-atoms with the silver cluster in the **S**-complex. Although the **V**-complex is more strongly bonded, the polarizability of the **S**-complex is more strongly affected due to these interactions. This is similar to what was found for the excitations described above.

Figure 4 presents the calculated real and imaginary polarizabilities in the wavelength range of 320−410 nm for both complexes. For comparison, the calculated real and imaginary polarizabilities for the Ag_{20} cluster are also included in the figures. The Ag_{20} cluster has an absorption maximum (maximum of the imaginary polarizability) at 360 nm, whereas for the two complexes the maxima are red-shifted slightly. For the **S**-complex, the shift is 5 nm, whereas a shift of 3 nm is found for the **V**-complex. The absorption peak for the **S**-complex is decreased and broadened, whereas a small increase is found for the **V**-complex but no change in the line width. For large silver nanoparticles, it is known that the surface plasmon is quite sensitive to the absorption of molecules onto the surface.[54−56] In general, a red shift of the plasmon peak is found, although a small blue shift at low coverage was attributed to charge-transfer interactions between the particle and the molecule.[55,56] The observation of a red shift is in good agreement with the results found here but the magnitude of the shift is much larger in the experiments (where the coverage is much higher). Since the smallest shift is found for the **V**-complex, one could relate this to a small blue shift due to charge-transfer interactions.

D. Enhanced Raman Scattering. As mentioned in the Introduction, three major contributions account for the observed huge enhancement. Although a clear-cut separation of these mechanisms is not possible, we will analyze three different aspects that correspond roughly to the categories mentioned above. In this section, we will discuss the effects of each individual mechanism on the Raman scattering intensities, and

(51) Dreuw, A.; Weisman, J. L.; Head-Gordon, M. *J. Chem. Phys.* **2003**, *119*, 2943−2946.
(52) Bonačić-Koutecký, V.; Fantucci, P.; Koutecký, J. *Chem. Rev.* **1991**, *91*, 1035−1108.
(53) Jensen, L.; Åstrand, P.-O.; Osted, A.; Kongsted, J.; Mikkelsen, K. V. *J. Chem. Phys.* **2002**, *116*, 4001−4010.
(54) Linnert, T.; Mulvaney, P.; Henglein, A. *J. Phys. Chem.* **1993**, *97*, 679−682.
(55) Malinsky, M. D.; Kelly, K. L.; Schatz, G. C.; Van Duyne, R. P. *J. Am. Chem. Soc.* **2001**, *123*, 1471−1482.
(56) Haes, A. J.; Zou, S.; Schatz, G. C.; Van Duyne, R. P. *J. Phys. Chem. B* **2004**, *108*, 6961−6968.

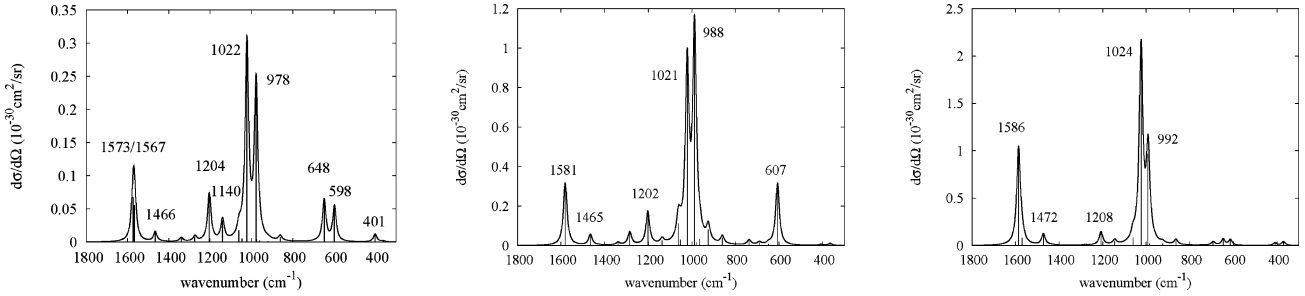

(a) Pyridine (b) **S**-complex (c) **V**-complex

Figure 5. Simulated normal Raman spectra of pyridine and the pyridine−Ag_{20} complexes at an incident wavelength of 514.5 nm based on static polarizability derivatives. Differential cross section in units 10^{-30} cm^2/sr and wavenumber in cm^{-1}. Spectra have been broadened by a Lorentzian having a width of 20 cm^{-1}.

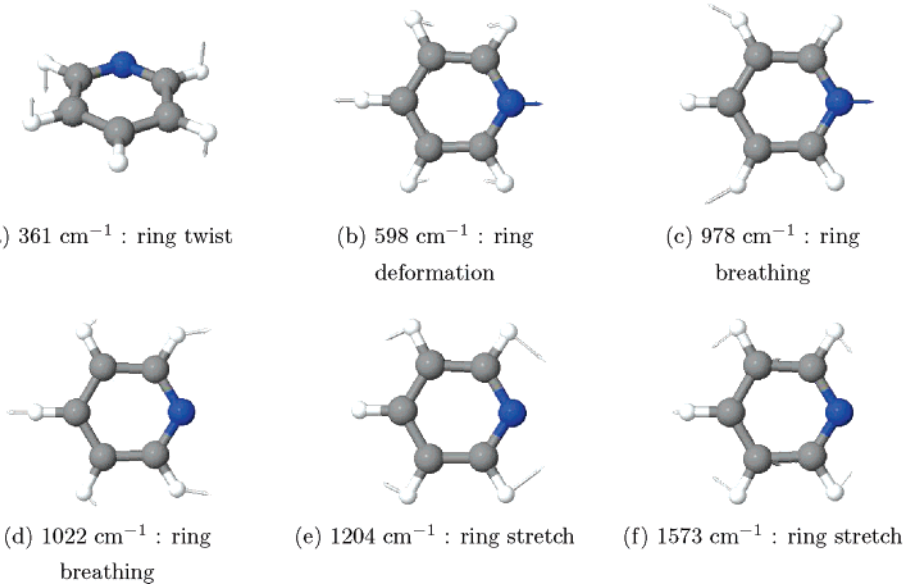

(a) 361 cm^{-1} : ring twist (b) 598 cm^{-1} : ring deformation (c) 978 cm^{-1} : ring breathing

(d) 1022 cm^{-1} : ring breathing (e) 1204 cm^{-1} : ring stretch (f) 1573 cm^{-1} : ring stretch

Figure 6. Normal modes of selected frequencies for pyridine.

we will term them as the "chemical enhancement", the "resonance enhancement", and the "electromagnetic enhancement".

1. Chemical Enhancement. It was shown above that the interactions between pyridine and the Ag_{20} cluster cause charge to be transferred from pyridine to the Ag_{20} cluster, thus leading to a change in the polarizability. These changes in the electronic properties of the molecule will affect its NRS spectra, as shown in the simulated NRS spectra presented in Figure 5 for wavenumbers between 300 and 1800 cm^{-1}. The polarizability derivatives needed in eq 1 were calculated at zero frequency; however, a wavelength of 514.5 nm was assumed for the calculations of the differential cross section. Normal modes for selected frequencies of pyridine important for the discussion are displayed in Figure 6.

We see that for pyridine alone, the NRS differential cross section is of the order of 10^{-31} cm^2/sr. The intensities are enhanced by about a factor of 4 for the **S**-complex and about a factor of 8 for the **V**-complex. The enhancement due to the chemical interaction is therefore of the order of 10. The fact that the **V**-complex shows larger enhancement is expected since it has a stronger bonding interaction compared to the **S**-complex, although the 598 cm^{-1} mode shows a larger enhancement for the **S**-complex. The NRS spectrum of pyridine is dominated by two intense peaks at 978 and 1022 cm^{-1}, both of which correspond to ring breathing modes. The relative intensities are sensitive to adsorption site, but we also found sensitivity to choice of functional, and thus it is properly not useful to assign physical significance to the results. Weaker peaks are found at 1573, 1567, 1204, 648, and 598 cm^{-1}. The harmonic frequencies are in good agreement with the experimental results;[57] however, the intensities of the weaker peaks are more intense in the simulated spectrum. Shifts in the harmonic frequencies are observed for both complexes, with the largest for the **V**-complex, which is again in agreement with the stronger bonding interaction for this complex. The largest shifts observed are for the modes at 1573 (ring stretch), 978 (ring breathing with N moving toward silver), and 598 cm^{-1} (ring deformation with N moving toward silver). The modes at 978 and 598 cm^{-1} involve vibrational motion of the N atom along the N−Ag bond, and the 1573 cm^{-1} mode consists mainly of C−C stretching with the α-carbon next to nitrogen vibrating toward the silver cluster. These modes are therefore expected to be influenced more by the interaction with the silver cluster. These observations are in line with the theoretical findings by Vivoni et al. on pyridine interacting with few atom silver clusters.[18]

Comparing the simulated spectra for the two complexes with that for pyridine, we see that overall they are quite similar. The

(57) Golab, J. T.; Sprague, J. R.; Carron, K. T.; Schatz, G. C.; Van Duyne, R. P. *J. Chem. Phys.* **1988**, *88*, 7942−7951.

most noticeable changes in the intensities are for the ring deformation modes found in pyridine at 648 and 598 cm^{-1}. For the **S**-complex only the symmetric ring deformation, shifted up to 607 cm^{-1}, is visible, whereas for the **V**-complex both modes are very weak. The ring breathing mode at 978 cm^{-1} is more enhanced than the mode at 1022 cm^{-1} for the **S**-complex, whereas the opposite is true for the **V**-complex. The differences between the two complexes are most likely linked to the different chemical environments of the hydrogens close to the N atom, since many of the modes involve motions of these hydrogens. This is particularly clear if one compares the deformation density depicted in Figure 2 and the normal modes in Figure 6.

2. CT Resonance Enhancement. In Raman scattering measurements where the wavelength of the radiation is close to an electronic excitation of the molecule, the intensity of the signal can be enhanced by a factor of up to 10^4-10^6. This process is referred to as resonance Raman scattering, and the enhancement is proportional to the oscillator strength of the transition. Depending on the nature of the interaction between a molecule and the metal cluster, additional metal−molecule CT states might be present. These new CT states can of course be at resonance with the radiation leading to enhanced Raman scattering. Among the different mechanisms contributing to the enhancements observed in SERS, the CT mechanism is probably the most controversial.[6] The main reason for this is the experimental difficulty in identifying the CT states and specific probing of this mechanism without the electromagnetic enhancement, although the work by Campion and co-workers[8,58] has shown that it is possible to identify the CT state and study the SERS spectrum if the transition is strong enough. The CT mechanism is often used to explain the dependence of certain bands in SERS experiments on the electrode potential.[22,59] The idea is that by changing the potential, the CT state can be tuned in to be at resonance or not. However, an alternative explanation is that a reorientation of the molecule relative to the surface occurs due to the changes in the electrode potential.[60]

As described above, evidence for a broad weak CT state for the pyridine−Ag system has been provided by EELS experiments.[47] Although the calculated CT states are in good agreement with the experimental observation, the states remain inconclusive due to the aforementioned problems with conventional TDDFT methods. However, since the CT states are separated in energy from the strong silver transitions, this allows us to probe the CT states directly. The simulated Raman scattering spectrum for the **S**-complex for an incident wavelength of 471 nm is presented in Figure 7. The wavelength of the incident light is chosen to be at resonance with the HOMO → LUMO + 1 CT excitation. This corresponds to the CT excitation with the largest oscillator strength and should result in the largest enhancements.

From Figure 7, we see that the intensities are of the order of 10^{-27} cm^2/sr, which corresponds to an enhancement of the order of 10^4 as compared to the NRS intensities of pyridine. Therefore, the enhancement due to resonance with the CT state gives an additional 3 orders of magnitude on top of the chemical

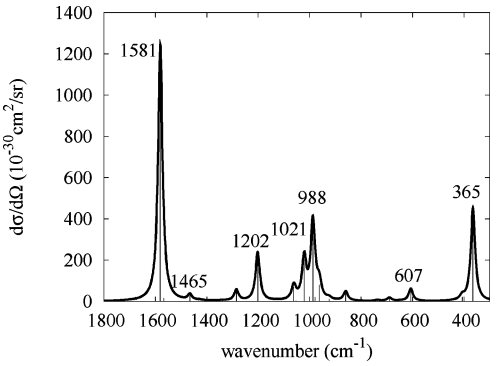

Figure 7. Simulated CT resonance-enhanced Raman spectrum for the **S**-complex at an incident wavelength of 471 nm. Differential cross section in units 10^{-30} cm^2/sr and wavenumber in cm^{-1}. Spectrum has been broadened by a Lorentzian having a width of 20 cm^{-1}.

enhancement. It is also clear that there are some quite significant changes in the CT resonance spectrum compared to the NRS spectrum in Figure 5. The ring stretch mode at 1581 cm^{-1} and the ring twist mode at 365 cm^{-1} show the largest enhancements and are now stronger than the two ring breathing modes around 1000 cm^{-1}. These two enhanced modes both involve motions of the atoms where the LUMO + 1 orbital (see Figure 3) is localized, which explains why these two modes are enhanced more than the rest. Experimentally, Arenas et al.[59] found that the modes at 598, 1204, and 1573 cm^{-1} show the strongest dependence on the electrode potential, with the mode at 1204 cm^{-1} showing the largest changes. Although we find that these modes are enhanced, the relative importance seems to be different. Arenas et al.[59] also analyzed the results theoretically by considering the displacements between the ground state of pyridine and its anion. Their relative intensities are in good agreement with the findings here, particularly the very strong enhancement of the mode at 1573 cm^{-1}.

3. Electromagnetic Enhancements. The simulated Raman scattering spectra for the **S**- and **V**-complexes at an incident wavelength of 365 and 363 nm, respectively, are displayed in Figure 8. The values for the incident light have been chosen so that they correspond with the peak values of the imaginary polarizability for the two complexes. The intensities are in the order of 10^{-25} and 10^{-26} cm^2/sr, which, compared to the NRS spectrum of pyridine, correspond to an enhancement of 10^6 and 10^5 for the **S**- and **V**-complexes, respectively. The additional enhancement due to resonances with the silver cluster is then around 10^4-10^5. For the **S**-complex, if we compare with its NRS spectrum, we see that the main changes are in the intensities but the spectrum looks quite similar. The modes at 607 and 988 cm^{-1} show the largest cross sections, and both are modes where the N atom moves toward the silver cluster. However, this is not the situation for the **V**-complex, where the spectrum looks quite different from its NRS spectrum. In particular, the large enhancement of the ring stretch mode at 1208 cm^{-1} makes this the most intense peak in the spectrum. This ring stretch mode has been found experimentally to be quite sensitive to the potential of the electrode,[59] which is usually explained in terms of either the CT mechanism or a reorientation effect. The strong dependence of the 1208 cm^{-1} mode on the binding site and the fact that it is not found to be very strong in the CT resonance spectrum support the latter explanation.

Last, we examine the Raman excitation profile for both **S**- and **V**-complexes (i.e., the changes in the intensity of the Raman

(58) Kambhampati, P.; Child, C. M.; Foster, M. C.; Campion, A. *J. Chem. Phys.* **1998**, *108*, 5013−5026.
(59) Arenas, J. F.; Tocón, I. L.; Otero, J. C.; Marcos, J. I. *J. Phys. Chem.* **1996**, *100*, 9254−9261.
(60) Moskovits, M.; DiLella, D. P.; Maynard, K. J. *Langmuir* **1988**, *4*, 67−76.

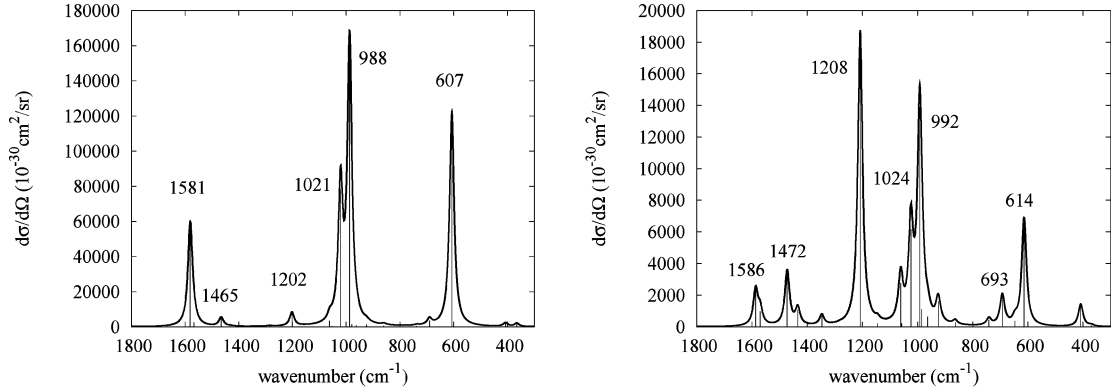

(a) **S**-complex (b) **V**-complex

Figure 8. Simulated electromagnetic-enhanced Raman spectra for the **S**- and **V**-complexes at an incident wavelength of 365 and 363 nm, respectively. Differential cross section in units 10^{-30} cm^2/sr and wavenumber in cm^{-1}. Spectra have been broadened by a Lorentzian having a width of 20 cm^{-1}.

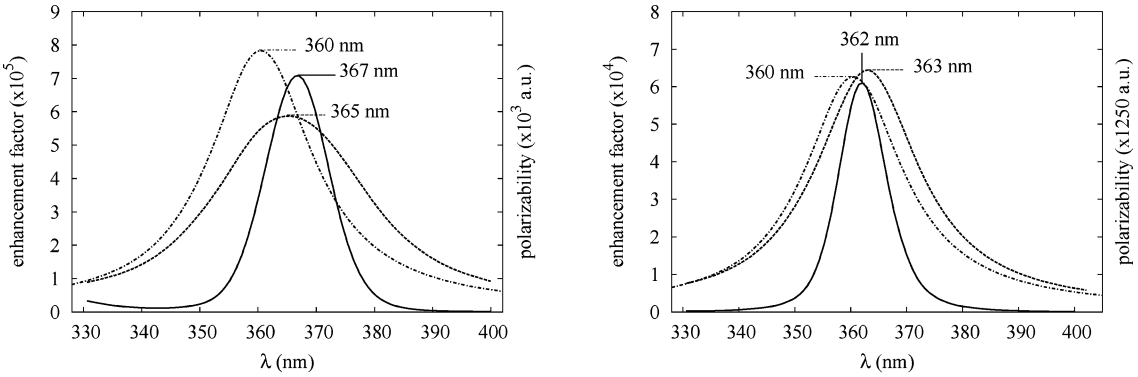

(a) **S**-complex (b) **V**-complex

Figure 9. Simulated Raman excitation profiles for the symmetric ring breathing mode of the two complexes. Enhancement factors are relative to the NRS value of pyridine and wavelength is in nanometers. Enhancement factors (solid line), imaginary polarizability of Ag_{20} (dashed−dotted line), and imaginary polarizability for the complex (dashed line).

scattering due to changes in the wavelength of the incident light). Experimentally, it is difficult to obtain the SERS excitation profile due to limited tunability of the laser frequencies. However, recent work by Van Duyne and co-workers has shown that this can be achieved in a detailed manner using nanosphere lithography.[61] Here we simulate the excitation profile for the symmetric ring breathing mode found at 988 and 992 cm^{-1} for the **S**- and **V**-complexes, respectively.

The simulated Raman excitation profiles are plotted in Figure 9. For comparison, the imaginary parts of the polarizabilities for both the Ag_{20} cluster and the Py−Ag_{20} complex are included in the figure as well. The excitation profile has been calculated for wavelengths between 330 and 400 nm. We see that the excitation profile is narrower than the absorption spectra as would be expected from the EM due to the $|E|^4$ enhancement in SERS. It is also broader for the **S**-complex compared to that for the **V**-complex. For the **S**-complex, the maximum enhancement occurs at 367 nm, which corresponds to a 7-nm red-shift compared to the Ag_{20} absorption maximum and a 2-nm red-shift compared to its absorption maximum. The maximum enhancement for the **V**-complex occurs at 362 nm, which is a red-shift of 2 nm from the absorption maximum of Ag_{20} but a blue-shift of 1 nm compared to the complex. For both complexes, the maximum enhancement is closer to the absorption maximum of the complex than that of Ag_{20}. The fact that the enhancement maximum does not coincide with the absorption maximum was also observed experimentally.[61] However, our use of the short-time approximation leads to a missing shift in the excitation profile relative to the absorption maximum due to the Stokes shift of the emitted photon (meaning that our calculation model the excitation profile for zero Stokes shift). As noted in ref 61, including for the Stokes shift makes the excitation spectrum blue-shifted relative to absorption.

IV. Conclusions

In this study, we have presented a detailed analysis of the enhanced Raman scattering of a pyridine−tetrahedral Ag_{20} model system using TDDFT. We have employed a recently developed approach based on a short-time approximation for the Raman cross section. This approach has allowed for a consistent treatment of both the EM and the chemical enhancements for this model system. The results show that both absolute and relative Raman intensities depend strongly on the local chemical environment of the molecule−metal binding site and on the incident excitation wavelength. An analysis of different contributions to the enhancements is presented, and the relative importance is in the following order: static chemical enhancements (factor of 10), charge-transfer enhancements (10^3), and EM enhancements (10^5). The calculated CT excitations are separated in energy from the strong silver absorption maximum.

(61) McFarland, A. D.; Young, M. A.; Dieringer, J. A.; Van Duyne, R. P. *J. Phys. Chem. B* **2005**, *109*, 11279−11285.

Therefore, the largest enhancement found (10^5-10^6) is due to the EM mechanism, with a small contribution from the chemical interaction. This suggests that the Raman scattering of molecules on a small cluster is enhanced in a way similar to that on nanoparticles. This observation of enhanced Raman scattering is in line with recent experiments by Dickson and co-workers,[10] although they find much larger enhancements. It still remains to be seen what enhancements will arise when the strong silver and CT excitations overlap. By combining information about the vibrational motion and the local chemical environment, we have been able to rationalize why certain normal modes are enhanced more than others.

Acknowledgment. We thank the Air Force Office of Scientific Research MURI program (F49620-02-1-0381) and DOD DURINT (F49620-01-1-0401).

Supporting Information Available: Tables containing optimized geometries and frequencies. This material is available free of charge via the Internet at http://pubs.acs.org.

JA0556326